The Journal of Supercritical Fluids 218 (2025) 106475

Contents lists available at ScienceDirect

The Journal of Supercritical Fluids

journal homepage: www.elsevier.com/locate/supflu

Complex phase behaviours related to gas injection in reservoir fluids

F.E. Benelli, G.O. Pisoni, M. Cismondi-Duarte *

Universidad Nacional de Córdoba. Facultad de Ciencias Exactas, Físicas y Naturales, Av. Vélez Sarsfield 1611, Córdoba, X5016GCA, Córdoba, Argentina
CONICET. Instituto de Investigación y Desarrollo en Ingeniería de Procesos y Química Aplicada (IPQA), Córdoba, Córdoba, Argentina

GRAPHICAL ABSTRACT

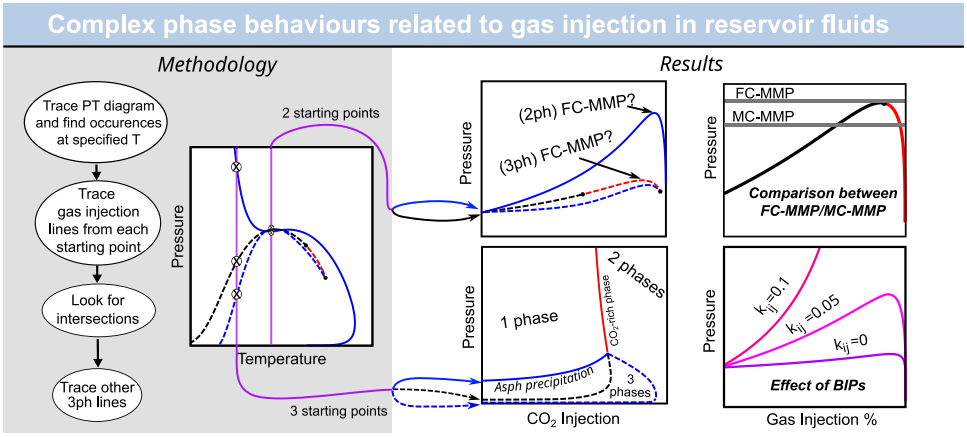

HIGHLIGHTS

- Calculation of isothermal phase diagrams for reservoir fluids with gas injection and three-phase regions.
- Effect of different gases injection on phase behaviour.
- Impact of key binary interaction parameters on predicted phase diagram and FC-MMP value.
- Effect and discussion of asphaltene precipitation on minimum miscibility pressure.

ARTICLE INFO

Keywords:
Gas injection
Reservoir fluids
Minimum miscibility pressure
Phase diagrams
Asphaltene onset pressure

ABSTRACT

Enhanced oil recovery (EOR) involves several techniques, including the injection of gas (such as natural gas, nitrogen, or CO_2) into the reservoir to increase its pressure, thereby displacing oil from one or more injection wells to production wells. For this process to be effective, it is essential that the injected gas and the oil reach a homogeneous state. Particularly, the First-Contact Minimum Miscibility Pressure (FC-MMP) offers a reliable (and safe) initial estimate for the pressure at which the EOR process should be conducted. In this work, an efficient algorithm is developed that allows computing complete pressure(P)-α diagrams (α: percentage of injected gas) at a fixed temperature using traditional cubic equations of state (EoS), including complex cases with three-phase regions. This algorithm is used to study both the qualitative and quantitative behaviour of the P-α diagrams and to analyse how FC-MMP changes with the injection of different gases or gas mixtures. Various reservoir fluids from the literature (with and without asphaltenes and with varying levels

* Corresponding author at: Universidad Nacional de Córdoba. Facultad de Ciencias Exactas, Físicas y Naturales, Av. Vélez Sarsfield 1611, Córdoba, X5016GCA, Córdoba, Argentina.
E-mail address: martin.cismondi@unc.edu.ar (M. Cismondi-Duarte).

https://doi.org/10.1016/j.supflu.2024.106475
Received 30 August 2024; Received in revised form 22 November 2024; Accepted 24 November 2024
Available online 3 December 2024

of CO_2 and methane) are evaluated. In one section, three injection gases are used: CO_2, N_2, and a synthetic natural gas mixture, comparing their effects on the P-α diagrams. Then, the impact of interaction parameters on phase equilibrium and FC-MMP is analysed, and the role of asphaltene precipitation is discussed. The study concludes with a quantitative comparison between the FC-MMP calculated here and the Multiple-Contact MMP (MC-MMP) reported for the same fluids. Additionally, the problem of whether asphaltenes precipitation should be considered or ignored in the determination of the FC-MMP is analysed and discussed, with different perspectives for conventional and non-conventional shale type reservoirs.

1. Introduction

Climate change is a well-established problem in the modern world, with constantly increasing global temperatures that can be problematic in the future. Carbon dioxide emissions can be identified as one of the main causes of climate change, with its increasing concentration in the atmosphere being of high concern. An important strategy to mitigate these problems is Carbon Capture, Utilisation and Storage (CCUS), where the residual carbon dioxide from some processes is utilised for other processes and finally stored to prevent it from reaching the atmosphere. In reservoir oil production EOR can be an excellent candidate for applying CCUS, using CO_2 as a displacement fluid during extraction and then storing it at the subsurface formations [1]. Another usage for CO_2 can be seen when depleted wells are used as underground natural gas reservoirs. In these cases, a layer of CO_2 can be used as a cushion of gas that assures that all the stored gas can be extracted later, making it easier to keep a smooth supply of natural gas during the whole year [2,3].

Currently, there are different techniques applied to EOR [4–6]. One of the most used, because it presents certain advantages over other techniques, is the injection of gas into the reservoir. This technique, which uses gases such as natural gas, nitrogen, or carbon dioxide (CO_2), accounts for nearly 60 percent of EOR production in the United States [7].

In EOR via miscible gas injection, a gas is injected from an injection well with two desired effects: maintain a high pressure to ease extraction and mix it with the entrapped oil, favouring its mobility and displacement [8]. During miscible gas EOR two driving forces occur before reaching miscibility, both of which usually happen simultaneously. On one side, a *vaporising drive* occurs when some molecules from the oil migrate to the gas phase until full miscibility is reached, while on the *condensing drive*, the oil becomes increasingly enriched with the injected gas components until both fluids are fully miscible. When performing EOR via miscible gas injection it is important to determine at which pressure both phases will be fully miscible, since this results in better production yields [9]. The minimum pressure needed to obtain a fully miscible system can be determined based on phase equilibria calculations. In this sense, different approaches can be taken to determine the minimum miscibility pressure (MMP). On one hand, the calculation of the MMP involving multiple contacts. In a multiple contact process the injection gas and reservoir fluid are mixed in successive and repeated contacts, this type of contact could be forward, backward, or a combination of both. Miscibility in injections develops when the phase compositions formed at each contact between the gas and the reservoir fluid move towards a critical point. The objective is to determine, for a given composition of the injection gas and the reservoir fluid (at the reservoir temperature), the specific critical point for those conditions [10]. It can be stated that the miscibility process of an injection gas with a reservoir fluid, in practice, is developed by a multiple contact process. Thus, the saturation pressure of a reservoir oil at a constant temperature, with a specified percentage of injected fluid, represents the full miscibility pressure under these conditions. When the pressure surpasses this value, the mixture achieves full miscibility. The maximum pressure value along the curve showing saturation pressure vs the second fluid's percentage is the First Contact Minimum Miscibility Pressure (FC-MMP). It is important to mention that the FC-MMP can give a conservative estimate of the pressure needed to obtain a fully miscible system since it will always be above the Multiple Contact Minimum Miscibility Pressure (MC-MMP) [10].

Dindoruk et al. [10] carried out an extensive review of the different techniques, both experimental and computational, to determine the MMP, in particular the MC-MMP. In the cited article, comparisons can be seen between analytical and experimental methods for real fluids (see [10]). There are several approaches to determine the MMP between a reservoir fluid and an injection gas. In particular, the determination of MC-MMP by calculation, using thermodynamic approaches, requires complex and tedious methods, which in many cases are inaccurate. Among them, the one proposed by Kaveh Ahmadi and Russell T. Johns [11] stands out. It proposes determining MC-MMP by a simpler and more precise method, which corrects the dispersion reported by other methods, and is also faster and less complicated, based on robust PT flash calculations that allow the use of any cubic equation of state (EOS).

On the other hand, the FC-MMP is easier to estimate considering it can be obtained from phase equilibria calculations at a fixed composition range, instead of simulation-based approaches like it is needed for MC-MMP [9,11,12]. Methods for calculating the FC-MMP have been presented by Jensen and Michelsen [13].

In another connection, when talking about MMP (either FC or MC), it may be important to consider the influence that asphaltene precipitation may have [14]. Nevertheless, as far as we know, consideration of this aspect is not present so far in the literature when dealing with phase behaviour involved in estimating FC-MMP values. Asphaltenes are the heaviest fraction of components in crude oil. They are usually defined based on their solubility, being the components that are completely soluble in aromatic solvents but insoluble in light paraffinic ones, like n-hexane and n-heptane [15]. This vague definition of asphaltenes makes them hard to identify and quantify in reservoir mixtures; their chemical composition and molecular structures are still discussed and not completely understood. Asphaltenes can be problematic in the continuous production of oil because they tend to precipitate and deposit on surfaces with changes in temperature, pressure or composition. This deposition can happen in all stages of oil production, from wellbore formations to refinery units. Asphaltene deposition can happen even when asphaltenes are present in really low concentrations so they can be seen as a possible problem that has no border [15]. In particular, considering oil production from porous media, asphaltenes can deposit in the porous media, resulting in a decrease in oil production [15]. Asphaltene precipitation can be modelled in different ways, being the use of Equations of State the most used approach, where the asphaltene precipitation is modelled as the appearance of a second liquid phase (incipient at an onset point) in addition to the saturated oil phase. When there is the presence of one or more substances that present high asymmetry with the rest of the system, like cases where there is carbon dioxide and heavy oil, three-phase equilibria may occur. Moreover, reservoir fluids that contain asphaltenes are very likely to present three-phase behaviour since they can precipitate as another phase besides the gas and oil [16,17]. The calculation of three-phase regions needs the inclusion of new variables and equations that represent the equilibria between the new third phase and the two already coexisting phases. When predicting phase behaviour with Equations of State there are multiple computation approaches that can be used, one of the most common being to perform

a sweep of flash calculations over a specific region to determine the coexistence of phases at each condition and locate the different boundaries between one, two and three-phase regions. While this approach can be simple and effective when not much information is known about the system, it also can be computationally intensive and give problems with convergence [18]. Other methodologies are focused on the calculation of phase boundary lines with efficient mathematical algorithms that assure easy convergence of points and also can avoid the need for stability analysis at each point. These methods can provide a phase diagram almost instantaneously, making it easier to explore the effect of different variables on phase equilibria. However, they require a carefully designed algorithmic strategy to locate and calculate each boundary line. Besides proposing an algorithmic strategy for tracing isothermal pressure-composition diagrams related to injection processes, this work tries to answer the following questions:

- What kind of phase behaviour can be observed when calculating the FC-MMP?
- Do all kinds of saturation lines have the same impact?
- Should asphaltene precipitation be considered in FC-MMP determination?

For this purpose, this work is organised in the different following sections: First, a new methodology to trace whole phase diagrams involving fluid injection is presented. The following section shows possible behaviours that can be seen when injecting different kinds of fluids, as well as the temperature effect. Another section is dedicated to illustrate the important effects that a proper tuning of some k_{ij} values may have on the $P\alpha$ diagrams, even if they do not affect the prediction of the reservoir fluid phase envelope. The last section compares the FC-MMP (calculated in this work) with the MC-MMP (taken from literature), showing how the former always presents higher values, with differences of varying magnitude.

2. Methodology

While the study of compositional effects in general on fluid phase behaviour is mathematically an open problem, with different possible degrees of freedom, the specific compositional variation involved in calculating the FC-MMP is limited to a single degree of freedom and is constrained to the relation between two fixed compositions, corresponding to the original fluid and the injected fluid. This relation can be specified with the inclusion of a new variable, defined as the molar relation between the amount of injected fluid and the sum of both fluids. The mole fraction of component i can then be defined in accordance with Eq. (1).

$$\mathbf{z}_i = \alpha \mathbf{z}_i^{inj} + (1-\alpha)\mathbf{z}_i^0 \tag{1}$$

Where $\mathbf{z}_i^{inj}$ and $\mathbf{z}_i^0$ are the mole fractions of component i in the injection fluid and original fluid, respectively. A common approach to obtain phase-boundary diagrams, especially when three-phase regions are considered, is to perform a sweep of flash calculations and stability tests in the region of interest, looking for the appearance and disappearance of different phases. While this method can be relatively easy to implement, flash calculations are computationally expensive and it can be problematic to obtain useful results due to failed convergence. All those challenges increase with the number of co-existing phases [18].

An alternative and already proven robust method is tracing the phase-boundary line, starting from an easy-to-converge point and following the line with an efficient numerical method. This method was first proposed by Michelsen [19], and extensively used by Cismondi-Duarte et al. [16,17,20–24]. Deiters, Nichita and Venkatarathnam [25–27] also proposed alternative procedures but with the same approach of tracing the line instead of doing phase-equilibrium calculations in a whole region. In this work we use a numerical continuation method as the ones used by previous works [16,17,28]. When tracing lines using these methods, the type and number of variables used will vary according to the number of phases present. In the case of two-phase lines, being one phase incipient, the variables include pressure and temperature in a logarithmic scale ($\ln P$, $\ln T$) and the K-factors that represent the ratio between the incipient and main phases mole fraction for each component, also in logarithmic scale.

$$K_i = \frac{\mathbf{y}_i}{\mathbf{z}_i} \tag{2}$$

When tracing three-phase boundaries, there are two phases already present in some molar proportion β with mole fractions x_i and y_i for each component i, respectively, and a new incipient phase with mole fractions w_i. These new mole fractions are conveniently related to the fluid global composition and two sets of K-factors that relate the equilibrium ratios between each main phase and this new incipient phase composition, as follows:

$$\mathbf{w}_i = \frac{\mathbf{z}_i}{\beta K_i^y + (1-\beta)K_i^x} \tag{3}$$

$$K_i^x = \frac{\mathbf{x}_i}{\mathbf{w}_i} \tag{4}$$

$$K_i^y = \frac{\mathbf{y}_i}{\mathbf{w}_i} \tag{5}$$

2.1. Analysis of how asphaltene behaviour varies according to the characteristics of the reservoir

In another work, Agger and Sørensen [28] have presented an algorithm used to trace PT and $P\alpha$ phase diagrams of reservoir fluids including asphaltenes precipitation using numerical continuation methods and stability analysis to detect three-phase regions. In this work, we use the same set of equations and method to trace phase boundary lines but with the difference that stability analysis is avoided by detecting double saturation points through lines intersection as shown in the previous works of Cismondi [16] and Benelli et al. [17] for three-phase diagrams calculation. Here we extend the same logic to cases of $P\alpha$ boundary lines using the information provided from an already obtained PT phase-diagram.

Our strategy for tracing complete $P\alpha$ phase diagrams can be summarised in four steps, which can be seen in Fig. 1:

PT three-phase diagram tracing Start with three-phase diagrams calculation, using the methodology already referenced [16,17].

Find occurrences Each PT phase-diagram line provides all the necessary information for a $P\alpha$ line to be started, since it corresponds to all the points where $\alpha = 0$. Therefore, with a selected temperature T we first locate the points in the previously calculated lines at that T value (including unstable sections of those lines). These points provide perfect initialisation for the $P\alpha$ lines, being already converged points. The two possible cases of starting points for $P\alpha$ lines can be seen at Fig. 2, where at high temperature there is a case with occurrences with two-phase regions, and at a lower temperature there are also occurrences with three phase regions.

Trace two-phase boundary $P\alpha$ lines With the previously converged point use the K and P values to initialise the $P\alpha$ line, which is calculated with the same equations as the original PT lines, just with the addition of the new balance Equation (Eq. (1)). This is repeated for each occurrence found at the specified temperature. The detailed methodology employed to trace lines and the complete sets of equations can be found in Appendix B.

Find three-phase regions Once two-phase boundary lines have been traced there is a range of possibilities to initialise three-phase regions:

Table 1
Selected fluids.

Fluid	CH_4 [%mol]	CO_2 [%mol]	Asphaltenes [%mol]	Model	References
A	17.5	1.7	0	PR76 [30]	[31]
B	27.36	11.4	0.3	SRK [32]	[9,33]
C	35.94[a]	2.4	0.8	PR78 [34]	[35,36]
D	20	0	0	PR78 [34]	[11,37]
E	35	0	0	PR78 [34]	[11,38]
F	34.1[a]	5.6[b]	0	PR78 [34]	[11,39]
G	37.1	6.6	0	PR78 [34]	[11,40]

[a] In this fluid characterisation CH_4 is lumped with N_2.
[b] In this fluid characterisation CO_2 is lumped with C_2H_6.

- There is an intersection (or more) between two lines calculated in the previous stage.
- A line intersects with itself.
- There is a three-phase line intersected at the specified T in the PT phase envelope i.e. at $\alpha = 0$.

In the first two cases, the intersections are known as Double Saturation Points (DSPs), where two incipient phases emerge from a saturated phase. A case with a DSP corresponding to the first situation can be seen at Fig. 3 where an Asphaltene Onset Line crosses with a bubble line, while another case in which a line intersects with itself is illustrated in Fig. 4. Three-phase line calculations can be initialised with the information provided with both lines at the intersection point. In the results section, Figs. 9b and 8a represent the complete phase diagrams including three-phase regions that correspond to the previously mentioned figures, respectively. On the other hand, there is always the possibility of a three-phase equilibrium region being already existent at $\alpha = 0$. In this case, the three-phase $P\alpha$ lines are initialised using the information provided with the already calculated three-phase PT lines, in particular the point(s) found at the specified temperature. A more complex fourth case which cannot be detected automatically by this algorithm, is the presence of an isolated three-phase region below the two-phase line, that appears after a certain amount of fluid injection, as it is shown by Coutinho et al. [29]. Since this region cannot be detected by lines intersection, the algorithm must be restarted with different initial values of α, starting from the corresponding PT envelope, where the isolated region will become the third possible case at the specified temperature.

2.2. Selected fluids

In this work, we selected a set of characterised fluids from different literature sources, including fluids with different characteristics, regarding for example the presence of asphaltenes. The selected fluids are listed and labelled in Table 1, while their complete compositions can be found in the supplementary material.

For fluids A and B, in Section 3 we analyse the obtained $P\alpha$ diagrams for three different injection gases, at 300 and 500 K:

- N_2
- CO_2
- Natural Gas ($0.8CH_4/0.15C_2H_6/0.05C_3H_8$)

In Section 4, Fluid C is used to provide a brief warning and analysis of how the different values of k_{ij} in a model can significantly impact the prediction of the FC-MMP for a given combination of reservoir fluid + injection gas. Finally, in Section 5, fluids D, E, F and G are used to make a comparison between MC-MMPs from the literature and FC-MMPs obtained with the algorithm described in this work.

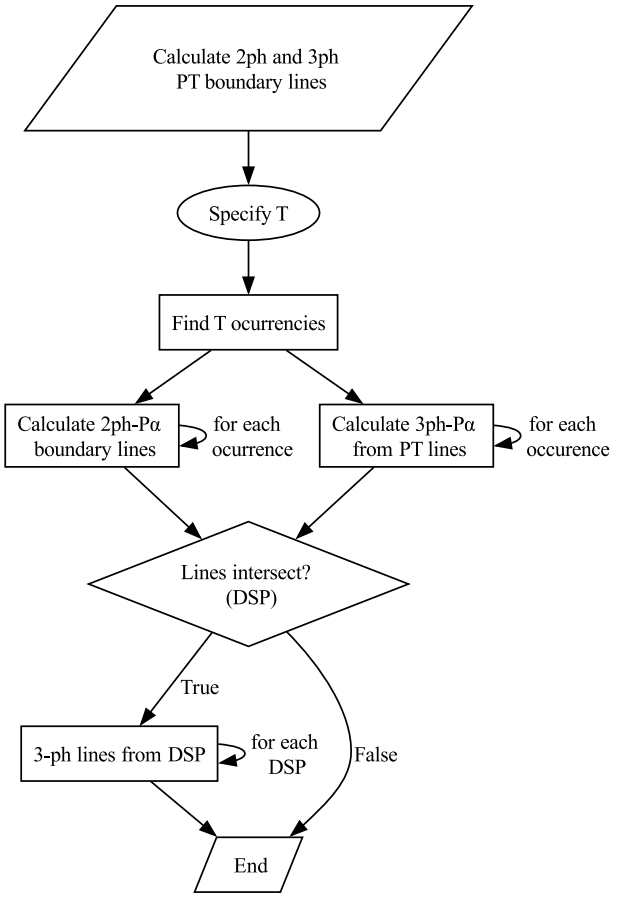

Fig. 1. Algorithm used for tracing $P\alpha$ lines.

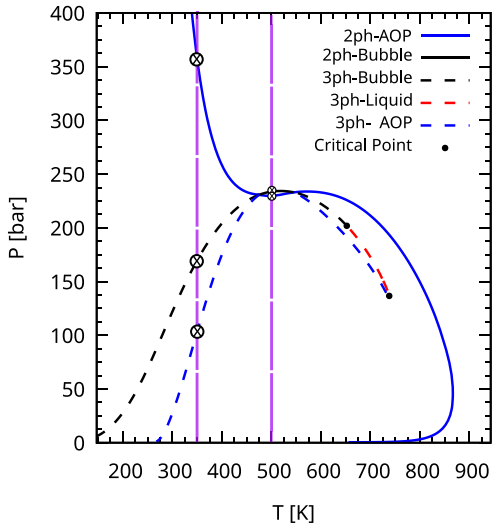

Fig. 2. Original PT phase diagram, showing found occurrences at $T = 350$ K and $T = 500$ K. In the region of the low-temperature three-phase bubble line, there is also an overlapping unstable bubble line that was not plotted to keep the visibility of the three-phase one.

3. Effect of different injection fluids on the FC-MMP and related diagrams

Here we present the results and analysis of the effects of different gas injections at different temperatures.

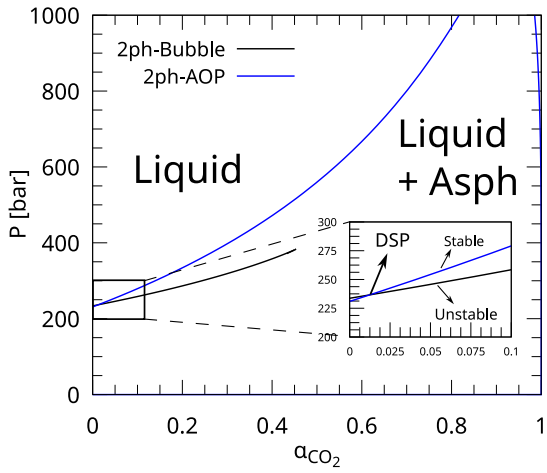

Fig. 3. Case with a DSP when tracing from the example case at $T = 500$ K. When zooming in it is possible to see that the two two-phase lines intersect each other in a DSP.

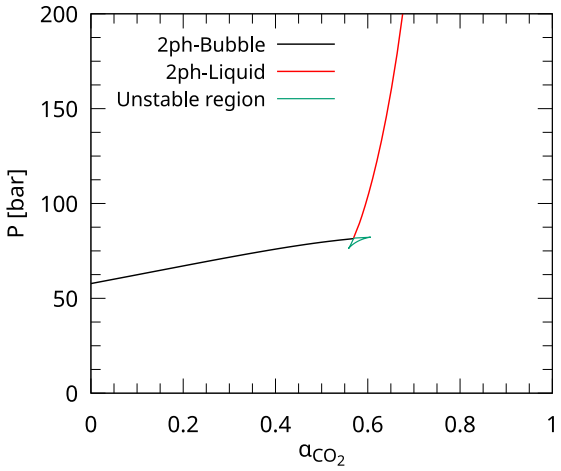

Fig. 4. Case of a two-phase boundary line that intersects itself in a DSP.

3.1. Effect of Nitrogen injection

While the injection of Nitrogen can be useful to increase oil extraction [41,42], it is possible to see that for Fluid A a FC-MMP is reached at extremely high pressures in most cases, especially at low temperatures (see Fig. 5). There are also cases where it is not even possible to find a value since phase separation remains open towards infinite pressure, like in the case with Fluid B (see Fig. 6). This behaviour can be expected, due to the high asymmetry (and very low miscibility) between nitrogen and the rest of the reservoir fluid components, being N_2 a diatomic molecule co-existing with long-chain alkanes, which favours phase-splitting instead of forming a miscible mixture.

A case where asphaltenes are taken into account in the fluid characterisation (Fluid B) can be seen in Fig. 6. Here two types of lines appear: upper AOPs (Asphaltene Onset Pressures) and lower AOPs. These lines represent the appearance or disappearance of an asphaltenic phase, being two-phase and three-phase boundary lines, respectively [16,17,28]. Between the upper and lower AOP lines, the three-phase incipient bubble line is present. In this fluid, the multi-phase regions increases monotonically with the amount of N_2 injected without reaching a maximum pressure.

In terms of the effect of temperature, it can be seen that at higher temperatures the phase-split regions reduce in size, with a bigger impact on the AOP lines. It is also possible to recognise the appearance of a critical point along the three-phase boundary at high pressure, where the incipient phase shifts from being the gas to the liquid phase.

At first, the absence of a FC-MMP on Fluid B could be seen as an effect of the presence of asphaltenes in the fluid characterisation since it is the main difference in comparison with the previous fluid. But, as seen in Fig. 7, if they are removed from the system the bubble line keeps being nearly the same.

3.2. Effect of Carbon Dioxide injection

In all the fluids studied, CO_2 injection has shown considerable sensitivity to temperature, where it is possible to see that, at low temperatures, FC-MMP cannot be observed due to an incipient liquid line that increases in pressure indefinitely. This behaviour can be explained by the asymmetry between CO_2 and the reservoir oil both in size and polarity, favouring the early formation of an incipient CO_2-rich liquid phase at temperatures around or below its critical temperature. While no full miscibility will be achieved at low temperatures, it is known that for high CO_2 percentages both phases will be rich in CO_2, with similar mobility properties, but one phase being richer in the heavy components and the other one on the light components [9]. This behaviour will not necessarily limit production, but it can be seen that, at lower pressures, there is the appearance of a third gas phase. This third phase could limit the production due to gas breakthrough. When moving to higher temperatures there is a transition of behaviour, where a FC-MMP is observed. This kind of behaviour is expected since the temperature is far above the critical temperature of CO_2.

In Fig. 9 we show the effect of CO_2 on Fluid B. A more complex behaviour is observed, where at low temperatures there is a DSP from which two three-phase boundary lines emerge, one corresponding to a CH_4-rich incipient phase and the other a lower AOP one. Compared to the previous fluid, we can see a similar behaviour where no FC-MMP can be observed at 300 K since a Liquid–Liquid equilibrium line goes to high pressures. Nevertheless, beyond that common point, Fig. 9a covers a much larger pressure range compared to Fig. 8a, presenting some particular more complex characteristics that need to be highlighted. First, note that the "3ph-Bubble" curve starts like that in the lower pressure range at $\alpha = 0$, but gradually changes to imply a liquid-like incipient phase as pressure increases. At the same time, that incipient phase gets richer and richer in CO_2 and therefore that line continues as the red "2ph-Liquid" line after passing the DSP, once the asphaltenes are completely solubilised in the main liquid. Accordingly, the three-phase region starts with a LLV character at low pressures, but suffers a continuous transformation towards LLL separation in the higher pressure region closer to the DSP. Second, note that the high-pressure part of the blue dashed-line departing from the DSP shows the paradox of actually representing upper instead of lower AOP's as its name indicates and is indeed the case in the low pressure part of Fig. 9a departing from $\alpha = 0$, as in all other figures in this work and the previous ones [16,17]. In accordance with that upper-AOP character, the curve is somehow continued to the left in the blue solid line, i.e. the standard upper-AOP curve, after passing the DSP, once no CO_2-rich phase is separated.

In the case of high temperature in Fig. 9b, and coming back to the FC-MMP perspective, both the AOP line and the three-phase boundary show a maximum in pressure. This behaviour with two different maxima (one on a two-phase upper AOP line and another on a three-phase line) can be a trigger for the question "Which of these two values should be considered the true FC-MMP?". One FC-MMP, the classic one, implies the end of two-phase separation, or a transition from one phase to two phases, while the other would correspond to a transition from two-phase to three-phase separation. To identify these two kinds of FC-MMP, we will denote them as (2ph)FC-MMP and (3ph)FC-MMP respectively. The question makes sense and deserves attention since, while the asphaltenes can be considered a separate phase from the main fluid, they might appear in a really small volumetric fraction as

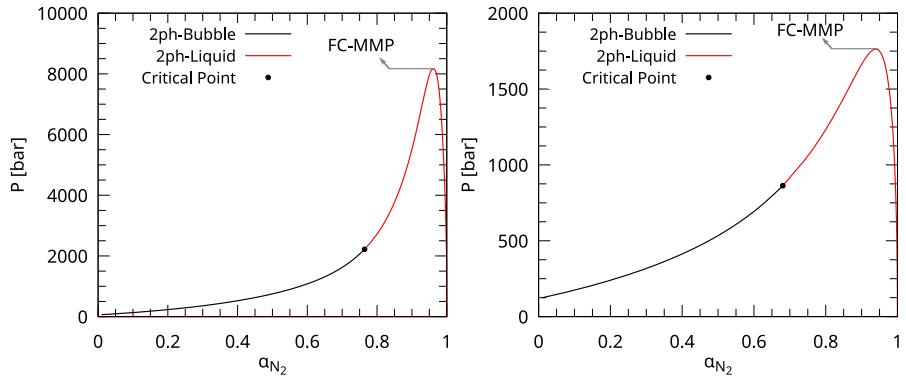

(a) $T = 300K$ (b) $T = 500K$

Fig. 5. Effect of N_2 injection on Fluid A.

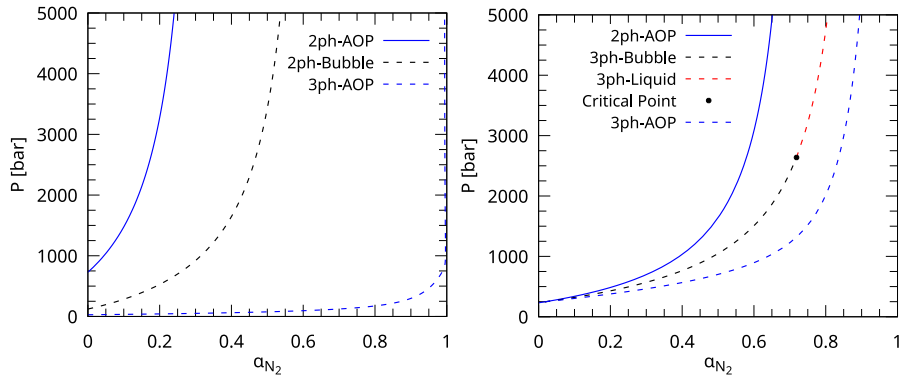

(a) $T = 300K$ (b) $T = 500K$

Fig. 6. Effect of N_2 injection on Fluid B.

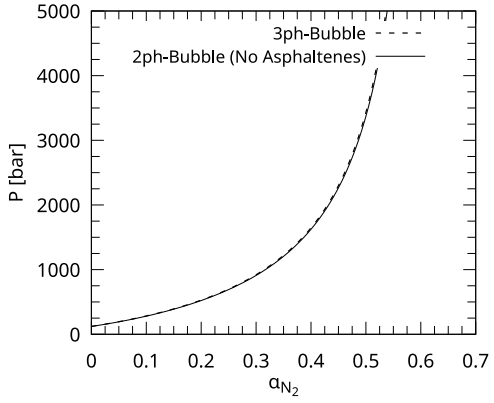

Fig. 7. Injection of N_2 on Fluid B at $T = 300$ K removing asphaltenes from the composition.

a dispersed phase. This makes us think that, in principle, the AOP line should not be taken into account for the determination of the FC-MMP, i.e. the (2ph)FC-MMP should be ignored, but instead use the maximum pressure from the three-phase equilibrium region, the (3ph)FC-MMP. Nevertheless, the work of Fakher and Imqam [43] suggests that asphaltene precipitation during CO_2 injection may cause a significant reduction in oil production in shale reservoirs where the asphaltenic phase can clog the porous rock, but with a lower impact in conventional reservoirs. Therefore, it might be important to consider the type of reservoir and in particular take the AOPs into account in cases of shales or similar rocks with very low porosity and permeability.

3.3. Effect of synthetic natural gas injection

In the case of Natural Gas (NG) injection it is possible to see in Fig. 10 that in Fluid A there is no appearance of a Liquid–Liquid line as seen in the case of CO_2 injection. This behaviour can be expected since the components of the NG mixture are already present in considerable amounts in the original fluid (and have better miscibility than CO_2 with the heavier components) so there is no significant increase of asymmetry in the system.

In the case of asphaltenes being present in the characterised fluid, the injection of NG negatively impacts the AOP line. It can be seen in Fig. 11 that the Upper AOP line increases to extremely high pressures, similar to the case of N_2 injection. However, in the three-phase region, there is a difference: unlike nitrogen injection, where the region remains open and continues to infinite pressures, this case exhibits a pressure maximum, i.e. a (3ph)FC-MMP and closes itself. It can also be seen that this behaviour is very similar to the two-phase behaviour of Fluid A with the same natural gas (omitting the Lower AOPs). Despite that similarity, this case with Fluid B shows how the injection of light gases destabilises the asphaltenes in the fluid, favouring their precipitation.

4. Importance of interaction parameters and their correct fitting

An EOS-based model should have reasonable default values for interaction parameters, which can then be adjusted depending on the parametric tuning strategy, to better depict the experimental behaviour of each fluid. If a model is fitted with a certain set of experimental points at some conditions and later used on other kinds of conditions, it might be inappropriate. For example, fitting interaction parameters

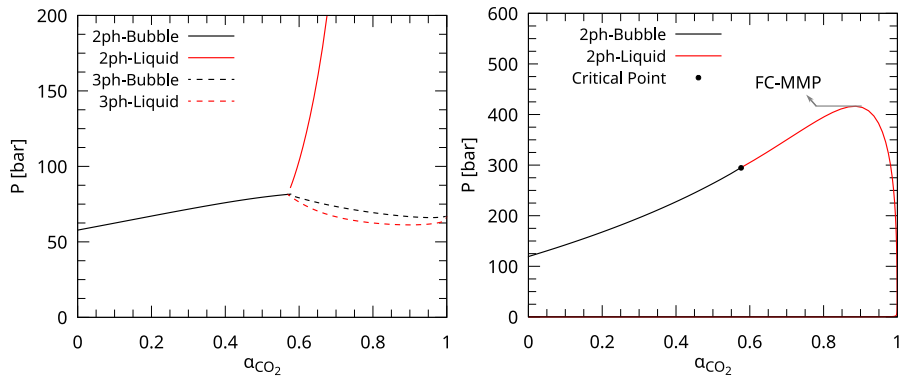

(a) $T = 300K$ (b) $T = 500K$

Fig. 8. Effect of CO_2 injection at different temperatures on Fluid A, the three-phase region was calculated automatically after detecting a DSP from a self-intersection of a line, as seen in Fig. 4.

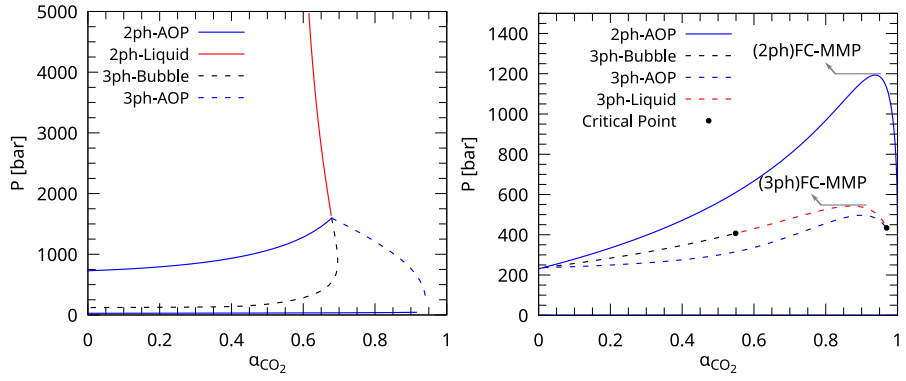

(a) $T = 300K$ (b) $T = 500K$

Fig. 9. Effect of CO_2 injection on Fluid B. The boundaries for each three-phase region were calculated after detecting a DSP from the intersection of two lines, as it can be seen on Fig. 3.

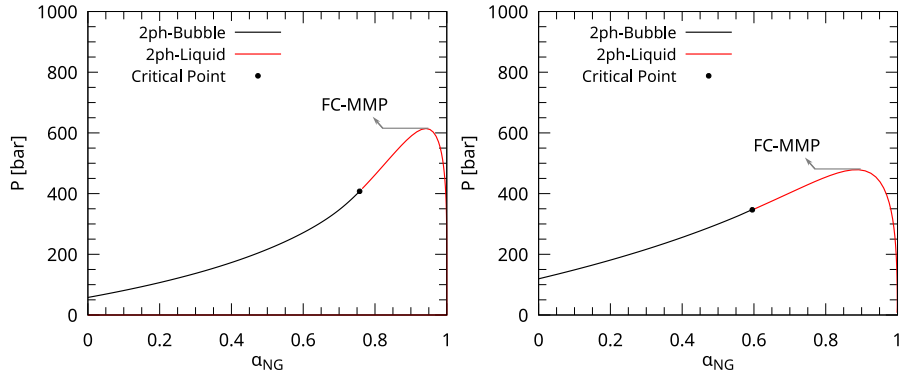

(a) $T = 300K$ (b) $T = 500K$

Fig. 10. Effect of NG injection on Fluid A.

using only points at a specific composition will not ensure that the model can correctly predict saturation points at other compositions. For one of the characterised fluids we already studied in previous works (Fluid C) [16,17], no k_{ij} values were provided between asphaltenes and CO_2 [36]. At first, a null k_{ij} might not be seen as a problem. As it can be seen in Fig. 12, this does not impact considerably on the calculated AOP, and this can be expected due to the low concentration of CO_2 in the original fluid. However, when considering the injection of CO_2, the impact of this parameter is more noticeable, as it is illustrated in Fig. 13.

It is well known that CO_2 destabilise asphaltenes, favouring their precipitation [15,44,45]. If we look at the effect of CO_2 injection on Fluid C on the PT phase diagram in 13a we can see that for temperatures above 390 K the asphaltenes precipitation happens earlier, at higher pressures. At lower temperatures, there would be an opposite effect, where higher concentrations of CO_2 prevent their precipitation.

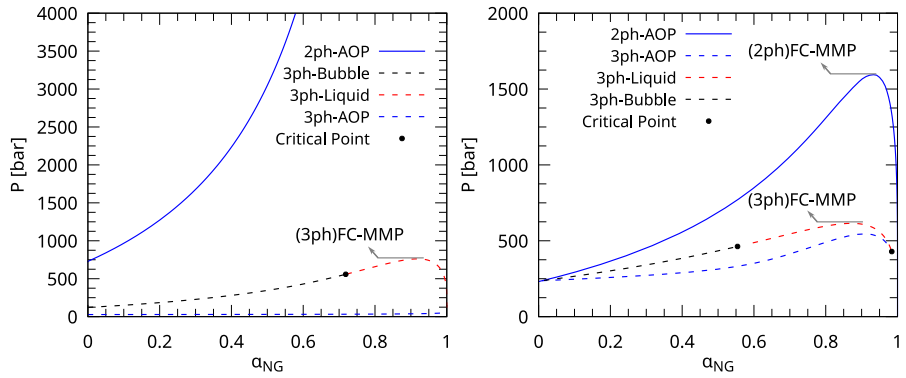

(a) $T = 300K$ (b) $T = 500K$

Fig. 11. Effect of NG injection on Fluid B.

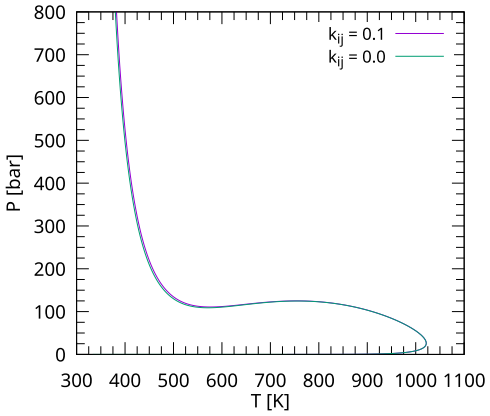

Fig. 12. Upper AOP lines of Fluid C with two different k_{ij} values between CO_2 and Asphaltene.

While we have not found any experimental evidence of this crossover behaviour, some works found it while modelling the phase behaviour of asphaltenes for specific fluids. When modelling with PC-SAFT Vargas et al. [46] observed this behaviour, denoting how CO_2 could stabilise the asphaltenes at lower temperatures. Regardless of which should be considered the real behaviour it is important to note that what can initially be seen as a minor change in behaviour, can cause a huge impact in predictions at different conditions. It can be more evident in Fig. 14 how CO_2 injection affects Upper AOPs depending on whether the temperature is above or below the crossover point.

As discussed in the previous paragraphs, it is expected that the k_{ij} value for CO_2-Asph will influence the (2ph)FC-MMP in a $P\alpha$ diagram. Fig. 15 illustrates the 2ph-AOP lines calculated for both zero and non-zero k_{ij} values. The impact is clearly evident: for a zero k_{ij}, the 2ph-AOP line indicates a (2ph)FC-MMP around 600 bar, whereas with an increase of k_{ij} the FC-MMP value also increases significantly. With a k_{ij} value of 0.05 the (2ph)FC-MMP presents a value of around 1400 bar and with a k_{ij} value of 0.1, the 2ph-AOP begins around 500 bar and monotonically rises in pressure as the CO_2 concentration reaches approximately 0.5, without presenting a (2ph)FC-MMP. Although not shown in Fig. 15, the (3ph)FC-MMP based on the bubble curve is practically insensitive to the same variations of k_{ij}.

5. Comparison between FC-MMP and MC-MMP

While MC-MMP calculations can give good approximations of the actual pressure that will be required to obtain full miscibility during enhanced oil recovery by miscible gas injection, FC-MMP can also provide a more conservative first estimate. This can be seen in Table 2, where in all cases FC-MMP is above the MMP reported by Ahmadi and Johns [11] with their multiple mixing cell algorithm. This behaviour is expected, since after each contact between the injection fluid and the reservoir oil, both fluids become more similar in composition due to molecules of the injection fluid being dissolved in the oil and some of the oil molecules being dissolved in the injection fluid. This process progressively reduces the compositional differences between both fluids, until full miscibility is achieved, if the pressure is high enough.

One important issue to consider in the analysis of these diagrams, in view of the previous discussion in Section 3.2 considering both (2ph) and (3ph)FC-MMP, is the following. AOP lines are not present in Fig. 16 simply because asphaltene content was not reported for cases 3 and 4 of Ahmadi and Johns (and by design is nonexistent for cases 1 and 2) and therefore there is no pseudo-compound representing asphaltenes in the EoS modelling for these cases. Nevertheless, based on the oils characteristics, it could well be that the original reservoir fluids contained indeed some low quantity of asphaltenes. Let us then suppose, just as an exercise with Case 3 of Ahmadi and Johns, that fluid F has an asphaltenes mole fraction of 0.001 and we decide to represent these asphaltenes by the same pseudo-compound used in fluid B, separating them from the heaviest pseudo compound in the original compositional Table "$C_7 + (5)$", which will now have a mole fraction of 0.046 instead of 0.047. The resulting phase diagram is presented in Fig. 17 as a variation of Fig. 16c. As expected, there is now an upper-AOP line at higher pressures, in this case with an extreme sensitivity to the gas injection, diverging rapidly to infinite pressure. But the location of the three-phase boundary which starts as a bubble pressure line in Fig. 17, seems to be essentially the same as that of the two-phase boundary in Fig. 16c. An explicit and detailed comparison in Fig. 18 shows that there are some differences, in particular some delayed increment of bubble pressures due to gas injection but then a higher maximum pressure in the curve. Nevertheless, the change in that maximum pressure value, which defines the FC-MMP, is not that important, around 7% in this case. Then, with the perspective discussed in Section 3, we may conclude that, at least for this range of low asphaltene contents, it would not have consequences to omit asphaltenes in the analysis of the MMP, as long as the reservoir has good porosity and permeability. However, asphaltenes should not be ignored if the flow is more restricted, like in shale or tight reservoirs.

6. Conclusions

A new methodology to trace phase diagrams with compositional variations, due to injection or mixing of fluids, has been proposed and implemented successfully. This methodology takes advantage of previously converged points in isoplethic diagrams, assuring a correct

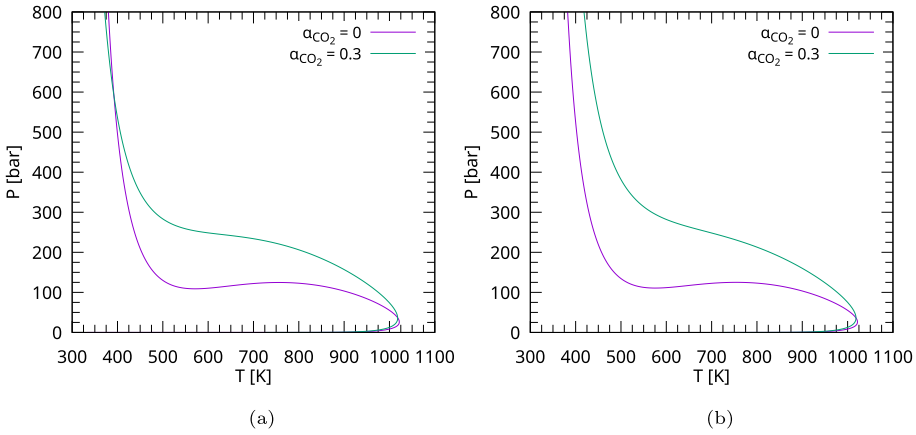

Fig. 13. Comparison of *PT* Upper AOP lines of Fluids C, at different levels of CO_2 injection. **a**: with $k_{CO_2-Asph} = 0$, it is possible to see the existence of a crossover point at T near 390 K. **b**: with $k_{CO_2-Asph} = 0.1$, there is no longer a crossover point.

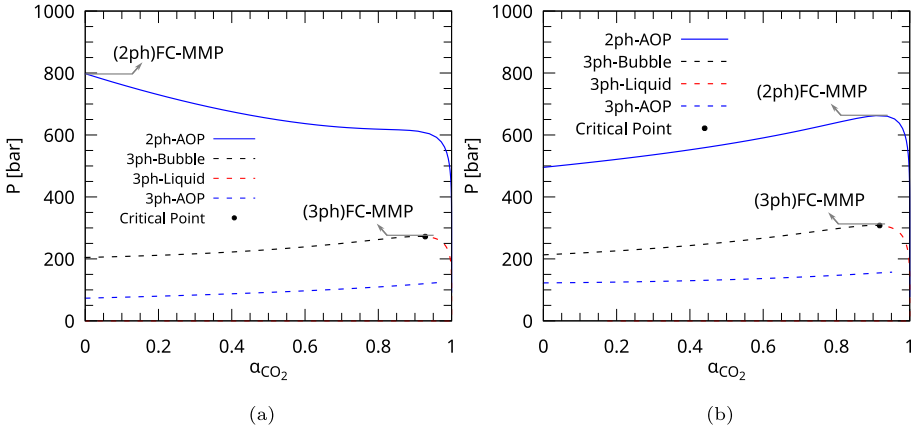

Fig. 14. Predicted phase diagrams when $k_{CO_2-Asph} = 0$. a: $T = 380$ K, where it is possible to see that the Upper AOP line goes down in pressure, meaning a stabilisation of asphaltenes by CO_2 injection. b: $T = 400$ K, where the Upper AOP line goes up in pressure, meaning a destabilisation by CO_2 injection.

Table 2
Differences between MC-MMP obtained by Ahmadi and Jones [11] and the FC-MMP obtained with the algorithm presented in this work. The fluid compositions can be seen at the supplementary material or in the referenced paper in [11].

Fluid	Injection gas CO_2 [%mol]	Temperature [K]	MC-MMP [bar]	FC-MMP [bar]	MC-MMP Depression [%]
D	80%	344.26	158.37	175.34	9.7
E	100%	322.04	89.49	127.32	29.7
F	12.4%[a]	373.15	228.56	326.72	30.0
G	17.75	358.15	215.46	417.23	48.4

[a] In this fluid characterisation the injection CO2 was lumped with ethane.

initialisation even on hard-to-converge regions like near critical points, and also of the detection of Double Saturation Points, which avoids the need to do stability analysis at each point.

The effect of different possible injection fluids on the phase behaviour of reservoir fluids has been studied and illustrated with specific cases, including the effect of this injection on possible asphaltene precipitation. Each injection fluid presented particular behaviours, where the size asymmetry between fluids shows a clear influence on the resulting immiscibility. In particular, small molecules like nitrogen and carbon dioxide present high FC-MMPs, if they even present one. For one of the fluids studied (Fluid B), no FC-MMP could be seen with nitrogen, not even at high temperatures like 500 K.

The injection of carbon dioxide and natural gas presented similar diagrams at high temperatures but, at lower ones like 300 K, carbon dioxide injection always shows the appearance of an incipient liquid phase rich in CO_2. This second liquid phase makes it impossible to obtain full miscibility on first contact, but it should be important to consider that this might not mean that a breakthrough could happen, and just two fluid phases flow along the reservoir.

When taking asphaltenes into the fluid characterisation, it is possible to observe two potential FC-MMPs, one of which is the absolute or rigorous FC-MMP at the maximum AOP, denoted (2ph)FC-MMP in this work, and another which is the maximum pressure of the three-phase region, the (3ph)FC-MMP. In conventional reservoirs with good porosity and permeability, the (2ph)FC-MMP based on AOP could be ignored in most cases since asphaltenes are known to be present in small quantities. This might not be the case when the EOR process happens in a shale reservoir, where the oil is in small nanopores that

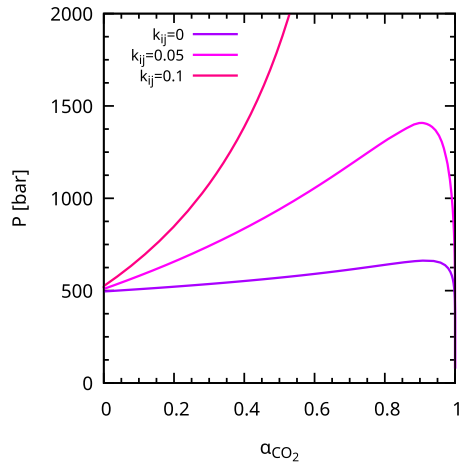

Fig. 15. AOPs of Fluid C at $T = 400$, with $k_{CO_2-Asph} = 0.0$, $k_{CO_2-Asph} = 0.05$ and $k_{CO_2-Asph} = 0.1$. It is possible to observe how, as the k_{ij} value increases, the AOP lines rise to higher pressures.

could be easily clogged by precipitated asphaltenes, even in small amounts.

In summary, the approach, the algorithmic strategy and the analysis presented in this work could help both researchers and application engineers dealing with MMP estimations or analysing complex phase behaviours related to gas injection. Specific adaptations and interpretations required to make practical decisions will depend on different factors, mainly the type of reservoir and operation, the gas to be injected and the asphaltene content in the reservoir fluid.

CRediT authorship contribution statement

F.E. Benelli: Writing – original draft, Visualization, Validation, Software, Methodology, Investigation, Data curation, Conceptualization. **G.O. Pisoni:** Writing – review & editing, Writing – original draft, Supervision, Investigation, Conceptualization. **M. Cismondi-Duarte:** Writing – review & editing, Writing – original draft, Supervision, Project administration, Methodology, Investigation, Funding acquisition, Conceptualization.

Declaration of competing interest

The authors declare that they have no known competing financial interests or personal relationships that could have appeared to influence the work reported in this paper.

Acknowledgements

Financial support from FONCyT, Argentina (PICT 2021–0008) is acknowledged. G.O.P. and M.C.D. are researchers from Consejo Nacional de Investigaciones Científicas y Técnicas (CONICET). F.E.B. is a research fellow of CONICET.

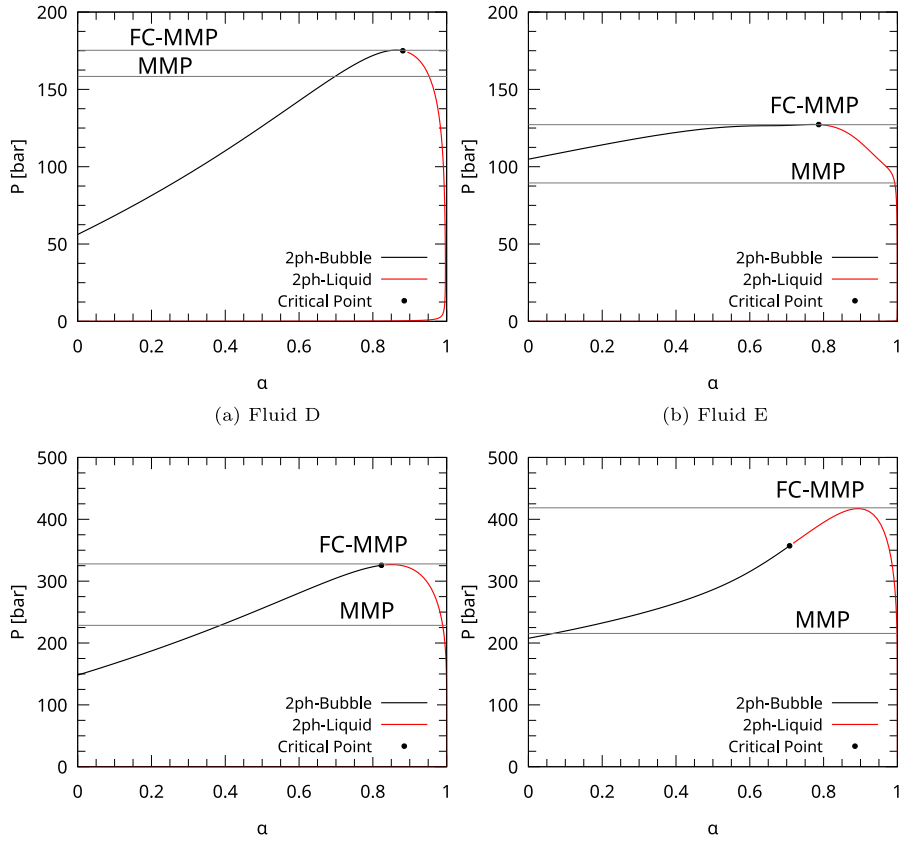

(a) Fluid D (b) Fluid E

(c) Fluid F (d) Fluid G

Fig. 16. Comparison between the FC-MMP obtained with the presented algorithm and the one obtained by the Multiple Mixing Cell algorithm presented by Ahmadi and Johns [11], fluids D to G correspond to cases 1 to 4 in the referenced paper [11].

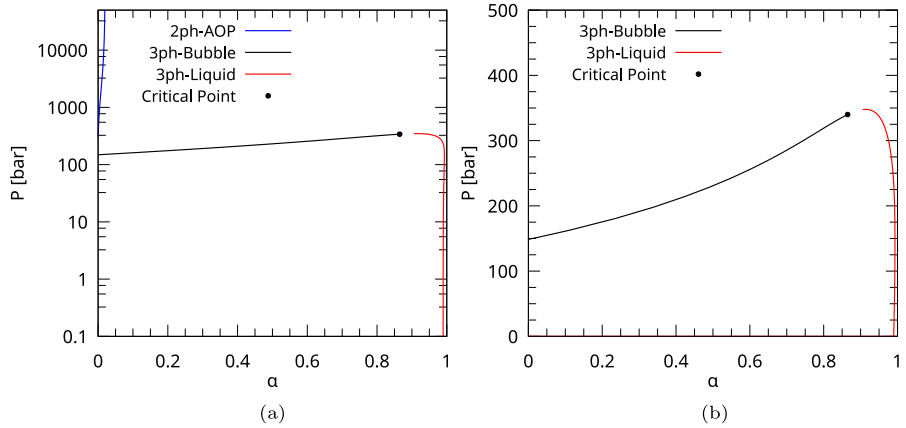

Fig. 17. Phase diagram of Fluid F when including asphaltenes in the characterisation. a: shows the full phase diagram on logarithmic scale. b: zoom on the three-phase region.

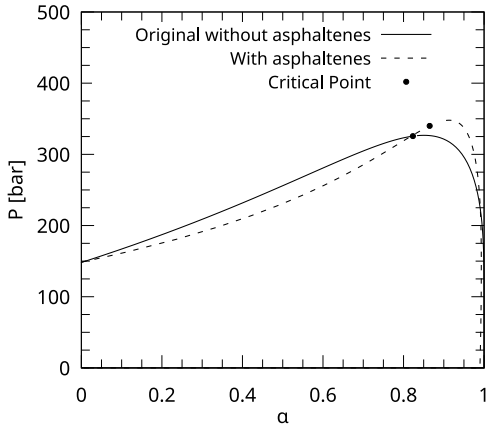

Fig. 18. Comparison between the phase diagram of the original fluid characterisation (two-phase line) and the line obtained when including asphaltenes (three-phase line).

Abbreviations and symbols

α Mole fraction of injected fluid

K_i Relation between mole fractions of component i in the incipient phase and in the main phase

K_i^x Relation between mole fractions of component i in phase x and the incipient phase

K_i^y Relation between mole fractions of component i in phase y and i in the incipient phase

x_i Mole fraction of component i in phase x

y_i Mole fraction of component i in phase y

w_i Mole fraction of component i in phase w

AOP Asphaltene Onset Pressure

Asph Asphaltenes

(2ph)FC-MMP two-phase First Contact Minimum Miscibility Pressure

(3ph)FC-MMP three-phase First Contact Minimum Miscibility Pressure

DSP Double Saturation Point

EoS Equation of State

EOR Enhanced Oil Recovery

FC-MMP First Contact Minimum Miscibility Pressure

MMP Minimum Miscibility Pressure

MC-MMP Multiple Contact Minimum Miscibility Pressure

P Pressure

T Pressure

Appendix A. Comparison with experimental data

This study employs the presented algorithm to make phase behaviour predictions during fluid injection. The algorithm relies on EoS models, previously fitted by other authors in the literature. Here, we evaluate the predictions of the fitted models using our algorithm, comparing the results with available experimental data, in order to demonstrate how the calculation of both scenarios can be achieved. Among the studied fluids, fluids A and B exhibit experimentally determined saturation points under gas injection conditions. As shown in Fig. A1, the model provides accurate predictions of the experimental data points. Similarly, Fig. A2 demonstrates good agreement with experimental bubble points, though slight deviations are observed in the AOPs. This suggests that AOPs with gas injection were not incorporated during the tuning of the EoS parameters.

Appendix B. Phase envelopes tracing methodology

Two-phase lines

The saturation point of a fluid after some injection of a second fluid on a molar proportion α, can be seen as the saturation point of a fluid of global composition $\mathbf{z}$ with an incipient phase of composition $\mathbf{y}$. The mole fractions $\mathbf{z}_i$ of the main phase are related to the mole fractions of the original fluid and the injection fluid by Eq. (1) of Section 2. Each saturation point can be obtained by solving the system of equations:

$$F(\vec{X}) = \begin{bmatrix} \ln K_1 + \ln \hat{\phi}_1^y(\mathbf{y}, P, T) - \ln \hat{\phi}_1^z(\mathbf{z}, P, T) \\ \vdots \\ \ln K_i + \ln \hat{\phi}_i^y(\mathbf{y}, P, T) - \ln \hat{\phi}_i^z(\mathbf{z}, P, T) \\ \vdots \\ \ln K_N + \ln \hat{\phi}_N^y(\mathbf{y}, P, T) - \ln \hat{\phi}_N^z(\mathbf{z}, P, T) \\ \sum_i^N (y_i - z_i) \end{bmatrix} = \vec{0} \tag{B.1}$$

Where N is the number of individual components present in the mixture. The first N equations correspond to the isofugacity criteria. The remaining equation corresponds to the mass balance.

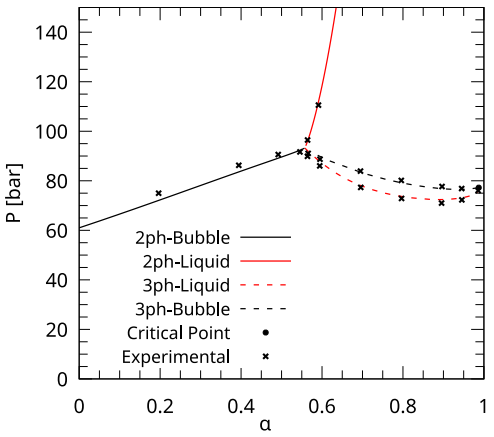

Fig. A1. Comparison of predicted lines with experimental values corresponding to the injection of CO_2 at $T = 307.59$ K into Fluid A. Experimental values and model from Khan et al. [31].

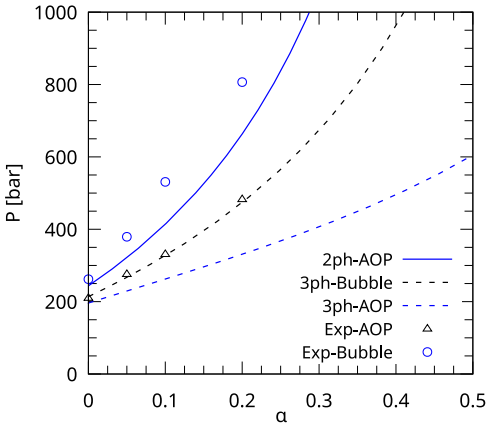

Fig. A2. Comparison of predicted lines with experimental values corresponding to the injection of N_2 at $T = 419.82$ K into fluid B. Experimental values from Jamaluddin et al. [33] and model from Pedersen and Christensen [9].

The corresponding variables are:

$$\vec{X} = \begin{bmatrix} \ln K_1 \\ \cdots \\ \ln K_i \\ \cdots \\ \ln K_N \\ \ln P \\ \alpha \end{bmatrix} \tag{B.2}$$

This leaves a system of $N+1$ equations and $N+2$ variables. Then, to solve the system of equations a specification equation is added:

$$X_{ns} - S = 0 \tag{B.3}$$

Where X_{ns} is one of the variables of the vector $\vec{X}$, being ns its position in the vector, and S is some specified value. For example, if ns= $N+1$ and $S = \ln(10)$, the system of equations specifies the variable $\ln P$ to a value of $\ln(10)$.

The whole system of equations can be solved with a Newton–Raphson method. While Eq. (1) is not visible on the system of equations, it does affect the global composition $\mathbf{z}$ which is an internal variable of the system and it must be considered for constructing the Jacobian matrix which, excluding the specification equation, is as in Box I.

For the last row of the Jacobian (corresponding to the specification equation) all values are 0 except on the position of the specified variable, where the value is 1.

The lines are started at a point easy to converge. Then, the next point is initialised with an extrapolation obtained from solving the following system for $\frac{dF}{dS}$:

$$\mathbf{J}\frac{d\vec{X}}{dS} + \frac{dF}{dS} = 0 \tag{B.5}$$

And later on extrapolating the previously converged point:

$$\vec{X}_{new} = \vec{X}_{converged} + \frac{d\vec{X}}{dS}\Delta S \tag{B.6}$$

Where ΔS, the step in the specified variable, can be updated after each solved point. Moreover, it is possible to change the specified variable for each new point to be calculated. Normally, the best choice is the variable corresponding to the highest value of $\frac{d\vec{X}}{dS}$.

Three-phase lines

Three-phase lines are calculated with the same methodology shown before for two-phase lines, but with an extended set of equations. Here we present the system of equations used to calculate three-phase lines. When two phases coexist in equilibrium on a molar proportion β and molar compositions $\mathbf{x}$ and $\mathbf{y}$, a third incipient phase with molar composition $\mathbf{w}$ might appear. The equilibrium factors involved in this type of saturation point were introduced in Section 2, Eqs. (4) and (5), while Eq. (3) shows how $\mathbf{w}$ depends of $\mathbf{z}$, K^x, K^y and β. Three-phase boundary lines can be calculated based on an extension of the system of equations presented for two-phase lines, as shown below (including the specification equation).

$$F(\vec{X}, S) = \begin{bmatrix} \ln K_1^x + \ln \hat{\phi}_1^x(\mathbf{x}, P, T) - \ln \hat{\phi}_1^w(\mathbf{w}, P, T) \\ \vdots \\ \ln K_i^x + \ln \hat{\phi}_i^x(\mathbf{x}, P, T) - \ln \hat{\phi}_i^w(\mathbf{w}, P, T) \\ \vdots \\ \ln K_N^x + \ln \hat{\phi}_N^x(\mathbf{x}, P, T) - \ln \hat{\phi}_N^w(\mathbf{w}, P, T) \\ \ln K_1^y + \ln \hat{\phi}_1^y(\mathbf{y}, P, T) - \ln \hat{\phi}_1^w(\mathbf{w}, P, T) \\ \vdots \\ \ln K_i^y + \ln \hat{\phi}_i^y(\mathbf{y}, P, T) - \ln \hat{\phi}_i^w(\mathbf{w}, P, T) \\ \vdots \\ \ln K_N^y + \ln \hat{\phi}_N^y(\mathbf{y}, P, T) - \ln \hat{\phi}_N^w(\mathbf{w}, P, T) \\ \sum_i^N (\mathbf{w}_i - 1) \\ \sum_i^N (\mathbf{x}_i - \mathbf{y}_i) \\ X_S - S \end{bmatrix} = \vec{0} \tag{B.7}$$

Where the corresponding variables are:

$$\vec{X} = \begin{bmatrix} \ln K_1^x \\ \cdots \\ \ln K_i^x \\ \cdots \\ \ln K_N^x \\ \ln K_1^y \\ \cdots \\ \ln K_i^y \\ \cdots \\ \ln K_N^y \\ \ln P \\ \alpha \\ \beta \end{bmatrix} \tag{B.8}$$

$$\mathbf{J}_{ij} = \begin{bmatrix} y_1 \frac{d\ln\phi_1^y}{dn_1} + 1 & \cdots & y_1 \frac{d\ln\phi_1^y}{dn_j} & \cdots & y_N \frac{d\ln\phi_1^y}{dn_N} & P\left(\frac{d\ln\phi_1^y}{dP} - \frac{d\ln\phi_1^z}{dP}\right) & \sum_k^N \left(K_k \frac{d\ln\phi_1^y}{dn_k}\right) \frac{d\mathbf{z}_1}{d\alpha} \\ \vdots & \ddots & \vdots & \ddots & \vdots & \vdots & \vdots \\ y_1 \frac{d\ln\phi_i^y}{dn_i} & \cdots & y_j \frac{d\ln\phi_i^y}{dn_j} + 1 & \cdots & y_N \frac{d\ln\phi_i^y}{dn_N} & P\left(\frac{d\ln\phi_i^y}{dP} - \frac{d\ln\phi_i^z}{dP}\right) & \sum_k^N \left(K_k \frac{d\ln\phi_i^y}{dn_k}\right) \frac{d\mathbf{z}_i}{d\alpha} \\ \vdots & \ddots & \vdots & \ddots & \vdots & \vdots & \vdots \\ y_1 \frac{d\ln\phi_N^y}{dn_N} & \cdots & y_j \frac{d\ln\phi_N^y}{dn_j} & \cdots & y_N \frac{d\ln\phi_N^y}{dn_N} + 1 & P\left(\frac{d\ln\phi_N^y}{dP} - \frac{d\ln\phi_N^z}{dP}\right) & \sum_k^N \left(K_k \frac{d\ln\phi_N^y}{dn_k}\right) \frac{d\mathbf{z}_N}{d\alpha} \\ y_1 & \cdots & y_j & \cdots & y_N & 0 & \sum_k^N \left[\left(K_k - 1\right) \frac{d\mathbf{z}_k}{d\alpha}\right] \end{bmatrix} \tag{B.4}$$

Box I.

For this system of equations the Jacobian Matrix is:

$$\mathbf{J}_{ij} = \frac{\partial F_i}{\partial \ln K_j^x} = K_j^x \left(\frac{d\ln\hat{\phi}_i^x}{dn_j} \frac{d\mathbf{x}_j}{dK_j^x} - \frac{d\ln\hat{\phi}_i^w}{dn_j} \frac{d\mathbf{w}_j}{dK_j^x} \right) + \delta_{ij} \text{ for } i,j \in [1,N] \tag{B.9}$$

Where δ_{ij} is the Kronecker delta.

$$\mathbf{J}_{i,N+j} = \frac{\partial F_i}{\partial \ln K_j^y} = K_j^y \left(\frac{d\ln\hat{\phi}_i^x}{dn_j} \frac{d\mathbf{x}_j}{dK_j^y} - \frac{d\ln\hat{\phi}_i^w}{dn_j} \frac{d\mathbf{w}_j}{dK_j^y} \right) \text{for } i,j \in [1,N] \tag{B.10}$$

$$\mathbf{J}_{i,2N+1} = \frac{\partial F_i}{\partial \ln P} = P\left(\frac{d\ln\hat{\phi}_i^x}{dP} - \frac{d\ln\hat{\phi}_i^w}{dP} \right) \text{ for } i,j \in [1,N] \tag{B.11}$$

$$\mathbf{J}_{i,2N+2} = \frac{\partial F_i}{\partial \alpha} = \sum_k^N \left[\frac{d\mathbf{w}_i}{d\alpha} \left(K_k^x \frac{d\ln\hat{\phi}_i^x}{dn_k} - \frac{d\ln\hat{\phi}_i^w}{dn_k} \right) \right] \text{ for } i,j \in [1,N] \tag{B.12}$$

$$\mathbf{J}_{i,2N+3} = \frac{\partial F_i}{\partial \beta} = \sum_k^N \left[\frac{d\mathbf{w}_i}{d\beta} \left(K_k^x \frac{d\ln\hat{\phi}_i^x}{dn_k} - \frac{d\ln\hat{\phi}_i^w}{dn_k} \right) \right] \text{ for } i \in [1,N] \tag{B.13}$$

$$\mathbf{J}_{N+i,j} = \frac{\partial F_{N+i,j}}{\partial \ln K_j^x} = K_j^x \left(\frac{d\ln\hat{\phi}_i^y}{dn_j} \frac{d\mathbf{y}_j}{dK_j^x} - \frac{d\ln\hat{\phi}_i^w}{dn_j} \frac{d\mathbf{w}_j}{dK_j^x} \right) \text{for } i,j \in [1,N] \tag{B.14}$$

$$\mathbf{J}_{N+i,N+j} = \frac{\partial F_{N+i}}{\partial \ln K_j^y} = K_j^y \left(\frac{\partial \ln\hat{\phi}_i^y}{\partial n_j} \frac{d\mathbf{y}_j}{dK_j^y} - \frac{d\ln\hat{\phi}_i^w}{dn_j} \frac{d\mathbf{w}_j}{dK_j^y} \right) + \delta_{ij} \text{ for } i,j \in [1,N] \tag{B.15}$$

$$\mathbf{J}_{N+i,2N+1} = \frac{\partial F_{i+N}}{\partial \ln P} = P\left(\frac{d\ln\hat{\phi}_i^y}{dP} - \frac{d\ln\hat{\phi}_i^w}{dP} \right) \text{ for } i,j \in [1,N] \tag{B.16}$$

$$\mathbf{J}_{N+i,2N+2} = \frac{\partial F_{i+N}}{\partial \alpha} = \sum_k^N \left[\frac{d\mathbf{w}_i}{d\alpha} \left(K_k^y \frac{d\ln\hat{\phi}_i^y}{dn_k} - \frac{d\ln\hat{\phi}_i^w}{dn_k} \right) \right] \text{ for } i \in [1,N] \tag{B.17}$$

$$\mathbf{J}_{N+i,2N+3} = \frac{\partial F_i}{\partial \beta} = \sum_k^N \left[\frac{\partial \mathbf{w}_i}{\partial \beta} \left(K_k^y \frac{\partial \ln\hat{\phi}_i^y}{dn_k} - \frac{\partial \ln\hat{\phi}_i^w}{\partial n_k} \right) \right] \text{ for } i \in [1,N] \tag{B.18}$$

$$\mathbf{J}_{2N+1,j} = \frac{\partial F_{2N+1}}{\partial \ln K_j^x} = K_j^x \frac{\partial \mathbf{w}_i}{\partial K_j^x} \text{ for } j \in [1,N] \tag{B.19}$$

$$\mathbf{J}_{2N+1,j+N} = \frac{\partial F_{2N+1}}{\partial \ln K_j^y} = K_j^y \frac{\partial \mathbf{w}_i}{\partial K_j^y} \text{ for } j \in [1,N] \tag{B.20}$$

$$\mathbf{J}_{2N+1,2N+1} = \frac{\partial F_{2N+1}}{\partial \ln P} = 0 \tag{B.21}$$

$$\mathbf{J}_{2N+1,2N+2} = \frac{\partial F_{2N+1}}{\partial \alpha} = \sum_i^N \frac{\partial \mathbf{w}_i}{\partial \alpha} \tag{B.22}$$

$$\mathbf{J}_{2N+1,2N+3} = \frac{\partial F_{2N+1}}{\partial \beta} = \sum_i^N \frac{\partial \mathbf{w}_i}{\partial \beta} \tag{B.23}$$

$$\mathbf{J}_{2N+2,j} = \frac{\partial F_{2N+2}}{\partial \ln K_j^x} = K_i^x \left(\frac{\partial \mathbf{x}_j}{\partial K_j^x} - \frac{\partial \mathbf{w}_j}{\partial K_j^x} \right) \tag{B.24}$$

$$\mathbf{J}_{2N+2,j+N} = \frac{\partial F_{2N+2}}{\partial \ln K_j^y} = K_i^x \left(\frac{\partial \mathbf{x}_j}{\partial K_j^y} - \frac{\partial \mathbf{y}_j}{\partial K_j^y} \right) \tag{B.25}$$

$$\mathbf{J}_{2N+2,2N+1} = \frac{\partial F_{2N+2}}{\partial \ln P} = 0 \tag{B.26}$$

$$\mathbf{J}_{2N+2,2N+2} = \frac{\partial F_{2N+2}}{\partial \alpha} = \sum_i^N \left[\frac{\partial \mathbf{w}_i}{\partial \alpha} \left(K_i^x - K_i^y \right) \right] \tag{B.27}$$

$$\mathbf{J}_{2N+2,2N+3} = \frac{\partial F_{2N+2}}{\partial \beta} = \sum_i^N \left[\frac{\partial \mathbf{w}_i}{\partial \beta} \left(K_i^x - K_i^y \right) \right] \tag{B.28}$$

$$\mathbf{J}_{2N+3,k} = \nabla F_{2N+3} = \delta_{k,ns} \text{ for } k \in [1, 2N+3] \tag{B.29}$$

Auxiliary derivatives

$$\frac{\partial \mathbf{z}_i}{\partial \alpha} = \mathbf{z}_i^{inj} - \mathbf{z}_i^0 \tag{B.30}$$

$$\frac{\partial \mathbf{w}_i}{\partial \alpha} = \frac{1}{\beta K_i^y + (1-\beta) K_i^x} \frac{\partial \mathbf{z}_i}{\partial \alpha} \tag{B.31}$$

$$\frac{\partial \mathbf{w}_i}{\partial \beta} = \mathbf{w}_i \frac{K_i^x - K_i^y}{(1-\beta) K_i^x + \beta K_i^y} \tag{B.32}$$

$$\frac{\partial \mathbf{w}_i}{\partial K_i^x} = -\mathbf{w}_i \frac{1-\beta}{(1-\beta) K_i^x + \beta K_i^y} \tag{B.33}$$

$$\frac{\partial \mathbf{x}_i}{\partial K_i^x} = K_i^x \frac{\partial \mathbf{w}_i}{\partial K_i^x} + \mathbf{w}_i \tag{B.34}$$

$$\frac{\partial \mathbf{y}_i}{\partial K_i^x} = K_i^y \frac{\partial \mathbf{w}_i}{\partial K_i^x} \tag{B.35}$$

$$\frac{\partial \mathbf{y}_i}{\partial K_i^y} = K_i^y \frac{\partial \mathbf{w}_i}{\partial K_i^y} + \mathbf{w}_i \tag{B.36}$$

$$\frac{\partial \mathbf{x}_i}{\partial K_i^y} = K_i^y \frac{\partial \mathbf{w}_i}{\partial K_i^y} \tag{B.37}$$

Appendix C. Supplementary data

Supplementary material related to this article can be found online at https://doi.org/10.1016/j.supflu.2024.106475.

Data availability

Data will be made available on request.

References

[1] Z. Chen, Y. Zhou, H. Li, A review of phase behavior mechanisms of CO2 EOR and storage in subsurface formations, Ind. Eng. Chem. Res. 61 (29) (2022) 10298–10318, http://dx.doi.org/10.1021/acs.iecr.2c00204.

[2] S. Shoushtari, H. Namdar, A. Jafari, Utilization of CO2 and N2 as cushion gas in underground gas storage process: A review, J. Energy Storage 67 (2023) 107596, http://dx.doi.org/10.1016/j.est.2023.107596.

[3] C. Cao, J. Liao, Z. Hou, H. Xu, F. Mehmood, X. Wu, Utilization of CO2 as cushion gas for depleted gas reservoir transformed gas storage reservoir, Energies 13 (3) (2020) 576, http://dx.doi.org/10.3390/en13030576.

[4] A. Gandomkar, R. Kharrat, Anionic surfactant adsorption through porous media in carbonate cores: An experimental study, Energy Sources A 35 (1) (2013) 58–65, http://dx.doi.org/10.1080/15567036.2010.501368, Publisher: Taylor & Francis.

[5] R. Kumar Pandey, A. Gandomkar, B. Vaferi, A. Kumar, F. Torabi, Supervised deep learning-based paradigm to screen the enhanced oil recovery scenarios, Sci. Rep. 13 (1) (2023) 4892, http://dx.doi.org/10.1038/s41598-023-32187-2, Publisher: Nature Publishing Group. URL https://www.nature.com/articles/s41598-023-32187-2.

[6] M. Motealleh, R. Kharrat, A. Gandomkar, H. Khanamiri, M. Nematzadeh, M. Ghazanfari, An experimental study on the applicability of water-alternating-CO2 injection in the secondary and tertiary recovery in one Iranian reservoir, Petrol. Sci. Technol. 30 (24) (2012) 2571–2581, http://dx.doi.org/10.1080/10916466.2010.514584, Publisher: Taylor & Francis.

[7] Enhanced oil recovery, 2024, https://www.energy.gov/fecm/enhanced-oil-recovery. (Accessed 21 August 2024).

[8] N.M.A. Hinai, A. Saeedi, N.M.A. Hinai, A. Saeedi, Miscible displacement oil recovery, in: Enhanced Oil Recovery - Selected Topics, IntechOpen, 2022, http://dx.doi.org/10.5772/intechopen.105757.

[9] K.S. Pedersen, J.A. Shaikh, P.L. Christensen, Phase behavior of petroleum reservoir fluids, CRC Press, 2014, http://dx.doi.org/10.1201/9781420018257.

[10] B. Dindoruk, R. Johns, F.M. Orr, Measurement of minimum miscibility pressure: A state of the art review, in: SPE Improved Oil Recovery Conference, Day 1 Mon, August 31, 2020, 2020, D011S016R001, http://dx.doi.org/10.2118/200462-MS, arXiv:https://onepetro.org/SPEIOR/proceedings-pdf/20IOR/1-20IOR/D011S016R001/2369859/spe-200462-ms.pdf.

[11] K. Ahmadi, R.T. Johns, Multiple-mixing-cell method for MMP calculations, SPE J. 16 (04) (2011) 733–742, http://dx.doi.org/10.2118/116823-PA.

[12] J.-N. Jaubert, L. Wolff, E. Neau, L. Avaullee, A very simple multiple mixing cell calculation to compute the minimum miscibility pressure whatever the displacement mechanism, Ind. Eng. Chem. Res. 37 (12) (1998) 4854–4859, http://dx.doi.org/10.1021/ie980348r.

[13] F. Jensen, M.L. Michelsen, Calculation of first contact and multiple contact minimum miscibility pressures, In Situ 14 (1) (1990) 1–17.

[14] A. Kariman Moghaddam, A.H. Saeedi Dehaghani, Modeling of asphaltene precipitation in calculation of minimum miscibility pressure, Ind. Eng. Chem. Res. 56 (25) (2017) 7375–7383, http://dx.doi.org/10.1021/acs.iecr.7b00613, Publisher: American Chemical Society.

[15] F.M. Vargas, M. Tavakkoli, Asphaltene deposition: fundamentals, prediction, prevention, and remediation, CRC Press, 2018, http://dx.doi.org/10.1201/9781315268866.

[16] M. Cismondi, Phase envelopes for reservoir fluids with asphaltene onset lines: An integral computation strategy for complex combinations of two- and three-phase behaviors, Energy Fuels 32 (3) (2018) 2742–2748, http://dx.doi.org/10.1021/acs.energyfuels.7b02790.

[17] F.E. Benelli, G.O. Pisoni, M. Cismondi-Duarte, A classification of phase envelopes for reservoir fluids with asphaltene onset lines: Exploring topology transitions based on compositional changes, Fluid Phase Equilib. 575 (2023) 113914, http://dx.doi.org/10.1016/j.fluid.2023.113914.

[18] S.E. Gorucu, R.T. Johns, Robustness of three-phase equilibrium calculations, J. Pet. Sci. Eng. 143 (2016) 72–85, http://dx.doi.org/10.1016/j.petrol.2016.02.025.

[19] M.L. Michelsen, Calculation of phase envelopes and critical points for multicomponent mixtures, Fluid Phase Equilib. 4 (1) (1980) 1–10, http://dx.doi.org/10.1016/0378-3812(80)80001-X.

[20] M. Cismondi, M. Michelsen, Automated calculation of complete Pxy and Txy diagrams for binary systems, Fluid Phase Equilib. 259 (2) (2007) 228–234, http://dx.doi.org/10.1016/j.fluid.2007.07.019.

[21] M. Cismondi, M.L. Michelsen, M.S. Zabaloy, Automated generation of phase diagrams for binary systems with azeotropic behavior, Ind. Eng. Chem. Res. 47 (23) (2008) 9728–9743, http://dx.doi.org/10.1021/ie8002914.

[22] M. Cismondi, M.L. Michelsen, Global phase equilibrium calculations: Critical lines, critical end points and liquid–liquid–vapour equilibrium in binary mixtures, J. Supercrit. Fluids 39 (3) (2007) 287–295, http://dx.doi.org/10.1016/j.supflu.2006.03.011.

[23] M. Cismondi, S.B. Rodriguez-Reartes, M.S. Zabaloy, Automated generation of isoplethic phase diagrams for fluid binary systems from equations of state, Fluid Phase Equilib. 571 (2023) 113821, http://dx.doi.org/10.1016/j.fluid.2023.113821.

[24] F.A. Sánchez, M. Cismondi Duarte, Calculation of critical endpoints and phase diagrams of highly asymmetric binary systems, J. Supercrit. Fluids 216 (2025) 106431, http://dx.doi.org/10.1016/j.supflu.2024.106431.

[25] U.K. Deiters, I.H. Bell, Calculation of phase envelopes of fluid mixtures through parametric marching, AIChE J. 65 (11) (2019) http://dx.doi.org/10.1002/aic.16730.

[26] D.V. Nichita, Density-based phase envelope construction, Fluid Phase Equilib. 478 (2018) 100–113, http://dx.doi.org/10.1016/j.fluid.2018.09.007, URL https://www.sciencedirect.com/science/article/pii/S037838121830387X.

[27] G. Venkatarathnam, Density marching method for calculating phase envelopes, Ind. Eng. Chem. Res. 53 (9) (2014) 3723–3730, http://dx.doi.org/10.1021/ie403633d.

[28] C.S. Agger, H. Sørensen, Algorithm for constructing complete asphaltene PT and Px phase diagrams, Ind. Eng. Chem. Res. 57 (1) (2018) 392–400, http://dx.doi.org/10.1021/acs.iecr.7b04246, Publisher: American Chemical Society.

[29] J.A.P. Coutinho, M. Jørgensen, E.H. Stenby, Predictions of three-phase regions in CO2-oil mixtures, J. Pet. Sci. Eng. 12 (3) (1995) 201–208, http://dx.doi.org/10.1016/0920-4105(94)00044-5.

[30] D.-Y. Peng, D.B. Robinson, A new two-constant equation of state, Ind. Eng. Chem. Fundam. 15 (1) (1976) 59–64, http://dx.doi.org/10.1021/i160057a011, Publisher: American Chemical Society.

[31] S.A. Khan, G.A. Pope, K. Sepehrnoori, Fluid Characterization of Three-Phase CO2/Oil Mixtures, OnePetro, 1992, http://dx.doi.org/10.2118/24130-MS.

[32] G. Soave, Equilibrium constants from a modified Redlich-Kwong equation of state, Chem. Eng. Sci. 27 (6) (1972) 1197–1203, http://dx.doi.org/10.1016/0009-2509(72)80096-4.

[33] A.K.M. Jamaluddin, N. Joshi, F. Iwere, O. Gurpinar, An Investigation of Asphaltene Instability Under Nitrogen Injection, OnePetro, 2002, http://dx.doi.org/10.2118/74393-MS.

[34] D.B. Robinson, The Characterization of the Heptanes and Heavier Fractions for the GPA Peng-Robinson Programs, Gas Processors Association, 1978.

[35] N.E. Burke, R.E. Hobbs, S.F. Kashou, Measurement and modeling of asphaltene precipitation (includes associated paper 23831), J. Pet. Technol. 42 (11) (1990) 1440–1446, http://dx.doi.org/10.2118/18273-PA.

[36] K. Gonzalez, H. Nasrabadi, M. Barrufet, Modeling asphaltene precipitation in a compositional reservoir simulator using three-phase equilibrium, J. Pet. Sci. Eng. 154 (2017) 602–611, http://dx.doi.org/10.1016/j.petrol.2016.09.010.

[37] R. Metcalfe, L. Yarborough, The effect of phase equilibria on the CO2 displacement mechanism, Soc. Petrol. Eng. J. 19 (04) (1979) 242–252, http://dx.doi.org/10.2118/7061-PA.

[38] F.M. Orr, R.T. Johns, B. Dindoruk, Development of miscibility in four-component CO2 floods, SPE Reserv. Eng. 8 (02) (1993) 135–142, http://dx.doi.org/10.2118/22637-PA.

[39] C.L. Hearn, C.H. Whitson, Evaluating Miscible and Immiscible Gas Injection in the Safah Field, Oman, OnePetro, 1995, http://dx.doi.org/10.2118/29115-MS.

[40] A.A. Zick, A Combined Condensing/Vaporizing Mechanism in the Displacement of Oil by Enriched Gases, OnePetro, 1986, http://dx.doi.org/10.2118/15493-MS.

[41] M. Almobarak, Z. Wu, D. Zhou, K. Fan, Y. Liu, Q. Xie, A review of chemical-assisted minimum miscibility pressure reduction in CO2 injection for enhanced oil recovery, Petroleum 7 (3) (2021) 245–253, http://dx.doi.org/10.1016/j.petlm.2021.01.001.

[42] O. Glasø, Miscible displacement: Recovery tests with nitrogen, SPE Reserv. Eng. 5 (01) (1990) 61–68, http://dx.doi.org/10.2118/17378-PA.

[43] S. Fakher, A. Imqam, Asphaltene precipitation and deposition during CO2 injection in nano shale pore structure and its impact on oil recovery, Fuel 237 (2019) 1029–1039, http://dx.doi.org/10.1016/j.fuel.2018.10.039.

[44] D.L. Gonzalez, F.M. Vargas, G.J. Hirasaki, W.G. Chapman, Modeling study of CO2-induced asphaltene precipitation, Energy Fuels 22 (2) (2008) 757–762, http://dx.doi.org/10.1021/ef700369u, Publisher: American Chemical Society.

[45] M. Jalili Darbandi Sofla, Z. Dermanaki Farahani, S. Ghorbanizadeh, H. Namdar, Experimental study of asphaltene deposition during CO2 and flue gas injection EOR methods employing a long core, Sci. Rep. 14 (1) (2024) 3772, http://dx.doi.org/10.1038/s41598-024-54395-0.

[46] F.M. Vargas, D.L. Gonzalez, G.J. Hirasaki, W.G. Chapman, Modeling asphaltene phase behavior in crude oil systems using the perturbed chain form of the statistical associating fluid theory (PC-SAFT) equation of state, Energy Fuels 23 (3) (2009) 1140–1146, http://dx.doi.org/10.1021/ef8006678, Publisher: American Chemical Society.